Atomistic Simulation of Poly(dimethylsiloxane) Permeability Properties to Gases and *n*-Alkanes

Zoi A. Makrodimitri and Ioannis G. Economou*

Molecular Thermodynamics and Modeling of Materials Laboratory, Institute of Physical Chemistry, National Center for Scientific Research "Demokritos", GR - 153 10 Aghia Paraskevi, Attikis, Greece

Received March 24, 2008; Revised Manuscript Received June 3, 2008

ABSTRACT: A recently developed atomistic force field for poly(dimethylsiloxane) (PDMS) is used to calculate the permeability properties of the polymer to light gases and to *n*-alkanes. The torsional potential barrier is re-estimated compared to the original force field. Chain dynamics and chain sizes are affected by this change while thermodynamic properties of the melt and of PDMS mixtures remain unaffected. The diffusion coefficients of penetrants to PDMS are calculated at different temperatures based on long molecular dynamics simulations. Subsequently, the permeability coefficients are estimated and ideal mixture selectivities are evaluated for binary hydrocarbon mixtures. In all cases, agreement with literature experimental data ranges from good to excellent. Calculations for mixed penetrant permeation reveal that, in the presence of a second penetrant species, solubility and diffusion coefficients increase, in agreement with recent experimental evidence.

1. Introduction

The accurate knowledge of the transport properties of polymeric materials based on their chemical structure is crucial for technological applications, since these properties govern the behavior of the materials at end-use conditions. For example, the accurate evaluation of the diffusion of small molecules dissolved in polymers influences the quality of a polymeric material used as a barrier (in food packaging, etc.). Typically, these properties are measured experimentally. Often though, experimental measurements are cumbersome and/or expensive. This is true for the measurement of the diffusion coefficients of penetrants in polymers in the low concentration limit and at high temperatures and pressures. In such cases, theoretical models or accurate computational approaches are preferred.

Considerable work has been devoted to the prediction of transport properties through theoretical models or detailed computer simulation studies. From the theoretical point of view, a model that describes accurately the diffusion of small molecules in polymers is the free volume theory of Vrentas and Duda.[1] This theory is based on the fundamental assumption of Cohen and Turnbull[2] that free volume redistribution is responsible for the molecular diffusion. Although widely used, for the accurate correlation of experimental data a number of system specific properties need to be fitted to the data.[3]

On the other hand, molecular dynamics (MD) simulations have been successfully used for the investigation of the molecular structure of membrane materials based on amorphous polymers and of the sorption and diffusion of low molecular weight penetrants in these materials.[4−12] In most of these studies, the diffusion coefficient of small gaseous penetrants, such as He, O_2, N_2, CH_4 and CO_2, in polymers was calculated. The duration of these MD simulations was limited to several hundred or few thousand ps. Diffusion coefficients of heavier penetrants in silicon rubbery polymers have been studied by Alentiev et al.[13] Harmandaris et al.[14] performed united atom (UA) atomistic MD simulations as well as coarse-grained MD simulations to predict elthylbenzene diffusion in polystyrene. Recently, Samios and co-workers[15] proposed a detailed methodology that allows quantitative analysis of diffusion jumps and the corresponding jumps frequency between neighboring cavities of gaseous alkanes, CH_4 through n-C_4H_{10}, permeating through heavy *n*-alkanes that can be easily applied to polymers.

Poly(dimethylsiloxane) (PDMS) is the most commonly used membrane material for separation of organic vapors and gases. The Si−O linkage of the backbone chain of PDMS is the structural feature which is responsible for the high chain flexibility of PDMS. This chain flexibility is reflected in the diffusion properties of penetrants in PDMS making this polymer very permeable. A number of MD simulations have been performed for the prediction of the diffusion coefficients of small penetrants in PDMS. In particular, Tamai et al.[8] used the UA approximation and performed 2−5 ns long MD simulations for the prediction of the diffusion coefficient of CH_4, H_2O and CH_2OH in PDMS. Charati and Stern[10] reported the diffusion coefficients of He, O_2, N_2, CO_2 and CH_4 in four silicon polymers, namely PDMS, poly(propylmethylsiloxane) (PPMS), poly(trifluoropropylmethylsiloxane) (PTFPMS) and (polyphenylmethylsiloxane) (PPhMS). In their work, each polymer chain was built from 10 repeat units and the mean-square displacements of penetrants were calculated from 200 ps trajectories of penetrant molecules. Sok and co-workers[7] executed short MD simulations (250 ps) and they estimated the diffusion coefficient of He and CH_4 in short PDMS chains. For both penetrants good agreement with experimental values was observed. Hofmann et al.[16] performed atomistic MD simulations for the investigation of the transport properties of different small molecules, including CH_4, H_2, O_2, N_2, H_2O and C_2H_5OH, in stiff chain glassy and flexible chain rubbery polymers (including PDMS). In all cases, the duration of the MD studies was up to 3 ns.

The main objective of this work is to extend diffusion and solubility studies to higher molecular weight penetrants in PDMS using an accurate UA force field and perform substantially long MD runs, on the order of 150 ns, in order to obtain reliable results. A wealth of experimental data have been reported on the solubility and diffusivity of light gases, *n*-alkanes, perfluoroalkanes and other compounds in PDMS at different temperatures and pressures,[17−30] and are used for the evaluation of simulation results.

Recently,[31] a UA force field was developed for the calculation of thermodynamic and structural properties of pure PDMS melts that was used subsequently for the prediction of infinite dilution solubility coefficients of light gases and *n*-alkanes in the polymer matrix. The agreement with experiment was very good in all

* Corresponding author. E-mail: economou@chem.demokritos.gr.

10.1021/ma800650u CCC: $40.75
Published on Web 07/03/2008

cases. Here, the focus is primarily on the calculation of the diffusion coefficient of gases and *n*-alkanes in PDMS at different temperatures. The torsional potential barrier of PDMS is revised, making the polymer chain more flexible. This modification has insignificant effect on the thermodynamic equilibrium properties of polymer melt and of polymer−penetrant mixtures while it affects chain dynamics and chain molecular size. Furthermore, it results in fair agreement between experimental data and simulation results for the diffusion coefficient of penetrants. Permeability coefficients as obtained from MD are compared to recent experimental data. Both pure- and mixed-penetrant systems are examined. The agreement between simulation and experiments is good in all cases.

2. Atomistic Force Field and Simulation Details

A UA description is used in this work to model the PDMS chains, according to which each carbon atom together with all hydrogens attached to it is considered as a single interaction site. In this force field, the potential energy function is written as the sum of contributions due to bond stretching, bond angle bending, dihedral angle torsion and nonbonded interactions between UAs in different chains or in the same chain but separated by more than three bonds. In PDMS, nonbonded interactions consist of short-range van der Waals repulsive and dispersive interactions modeled with the Lennard-Jones potential and long-range electrostatic (Coulombic) interactions modeled using the reaction field method.[32] The functional form of the force field in terms of the potential energy is:

$$V_{\text{total}}(\mathbf{r}_1, ..., \mathbf{r}_N) = V_{\text{stretching}} + V_{\text{bending}} + V_{\text{torsion}} + V_{\text{non-bonded}} = \sum_{\text{all bonds}} V(l_i) + \sum_{\text{all bond angles}} V(\theta_i) + \sum_{\text{all torsional angles}} V(\phi_i) + \sum_{\text{all pairs}} V(r_{ij}) = \sum_{\text{all bonds}} \frac{k_{l_i}}{2}(l_i - l_{i,o})^2 + \sum_{\text{all bond angles}} \frac{k_{\theta_i}}{2}(\theta_i - \theta_{i,o})^2 + \sum_{\text{all torsional angles}} \frac{1}{2}k_{\phi_i}(1 - \cos 3\phi_i) + \sum_{\text{all pairs}} \left(4\varepsilon_{ij}\left[\left(\frac{\sigma_{ij}}{r_{ij}}\right)^{12} - \left(\frac{\sigma_{ij}}{r_{ij}}\right)^{6}\right] + \frac{q_i q_j}{4\pi\varepsilon_o}\left(\frac{1}{r_{ij}} + \frac{(\varepsilon_s - 1){r_{ij}}^2}{(2\varepsilon_s + 1){r_c}^3}\right)\right) \quad (1)$$

where l_i, θ_i and ϕ_i denote bond length, bond angle and torsional angle respectively, r_{ij} is the distance between interaction sites i and j and q_i is the partial charge on site i. Subscript o denotes parameter value at equilibrium. Flexible bonds are used and the potential energy of each bond is evaluated by using a simple harmonic potential (first term on the rhs of eq. 1). Similarly, bond-angle fluctuations around the equilibrium angle are subject to harmonic fluctuations (second term on the rhs of eq 1). For all dihedral angles, a 3-fold symmetric torsional potential is used where k_{ϕ_i} is a force constant that measures chain flexibility and $\phi = 0°$ denotes a *trans* state (third term on the rhs of eq 1). Here there is only one type of torsional angle so $k_\phi = k_{\phi_i}$. In eq 1, ε_s is the dielectric constant of solvent, ε_o is the dielectric permittivity of vacuum (equal to 8.85419×10^{-12} C^2 J^{-1} m^{-1}) and r_c is the cutoff distance for the electrostatic interactions. Standard Lorentz−Berthelot combining rules are used to describe nonbonded Lennard-Jones interactions between sites of different type:

$$\varepsilon_{ij} = \sqrt{\varepsilon_{ii}\varepsilon_{jj}} \text{ and } \sigma_{ij} = \frac{\sigma_{ii} + \sigma_{jj}}{2} \quad (2)$$

In our previous work,[31] the force field for PDMS was applied to predict the structure and thermodynamic properties of the polymer melt in different temperatures and pressures. The starting point for the force field parametrization was the model proposed by Sok et al.[7] The Lennard-Jones parameters for CH_3 were modified in order to obtain good agreement with experimental data over the entire range of conditions. The new parameter set was used subsequently for the prediction of solubility of gases and liquids in PDMS.

Current work focuses primarily on transport properties and more specifically on the diffusion coefficient of small molecules in the polymer. The polymer chain flexibility and the free volume distribution affect significantly these properties. In this respect, k_ϕ is the primary force field parameter that controls these structural characteristics. Consequently, in this work we used two different k_ϕ values, namely k_ϕ= 1.8 kcal/mol (as in ref 31 based on an earlier model by Sok et al.[7] and will be referred to as Model I) and k_ϕ= 0.9 kcal/mol, that is a 50% reduction over Model I, and will be referred to as Model II. All the remaining force field parameters remain unchanged compared to ref 31.

MD simulations were performed at the isobaric−isothermal (*NPT*) ensemble using Nosé and Klein extended method[33] and at the canonical (*NVT*) ensemble. In *NPT* simulations, an integration time step of 0.5 fs and the fifth order Gear predictor-corrector scheme[34] were used to integrate the equations of motion in Cartesian coordinates. The values of the parameters W and Q in the Langragian form of the extended method were the same with those of previous work in PDMS.[31] *NVT* simulations were performed for the estimation of the diffusion coefficient of light gases and *n*-alkanes in PDMS matrix. In these simulations, an increased time step of 2 fs was used and the equations of motion were solved using the velocity Verlet algorithm.[32] In all cases, to maintain the temperature fixed at its prescribed value, the Berendsen thermostat[35] was used with coupling constant equal to 0.1 ps. Simulations were performed in machines based on Intel Xeon CPU 2.8 GHz processor. For the systems under investigation, 1 ns of simulated time corresponds to approximately 7 h of computing time.

All PDMS simulation boxes consisted of 3 chains of 80 monomer units each. For such a system, the average edge length of the cubic box was 32 Å. The initial configurations were obtained using the Cerius[2] software package of Accelrys Inc. Polymer chains were built in an amorphous cell using periodic boundary conditions. These initial configurations were subjected to molecular mechanics.[36] Energy minimization took place in two stages. First, the steepest descent method was used with a maximum number of iterations equal to 100 followed by the conjugate gradient method with a maximum number of iterations up to 10 000. In all simulations, periodic boundary conditions were applied to the simulation box. A Verlet neighbor list[32] and a truncated Lennard-Jones and electrostatic potential were used to speed up calculations of interactions between molecules. In this work, the Lennard-Jones potential tail beyond $r = 1.45\sigma$ was substituted by a fifth order polynomial, whose value beyond $r = 2.33\sigma$ is equal to zero. For electrostatic interactions, the cutoff distance, r_c, was equal to 13.5 Å, a value which is smaller than half the box edge length. The dielectric constant of solvent, ε_s, was chosen to be 2.8, which is the static value for PDMS. The instantaneous pressure of the system P_{int} was calculated during the simulation according to the molecular virial expression proposed by Theodorou et al.[37] The "tail" contributions to the internal energy and to the pressure were taken into account.[32]

For the evaluation of the chemical potential of light gases and *n*-alkanes in PDMS, *NPT* simulation runs of 6 ns were performed; the first nanosecond corresponded to the "equilibration" stage and the remaining 5 ns to the "production" stage where instantaneous properties are averaged. In order to improve statistics in the calculated solubility properties, for each state point four runs were performed starting from completely independent different initial configurations. In each simulation

run, 5000 configurations were recorded at equal time intervals. These configurations were used for the calculation of the excess chemical potential of light gases and *n*-alkanes in PDMS using the Widom test particle insertion method.[38] According to Widom's method, the chemical potential is calculated from the ratio of the partition function of a system containing $N + 1$ molecules divided by the partition function of a system containing N molecules, where both systems are under the same temperature and volume or pressure conditions. The "ghost" molecule is inserted randomly into the simulated system. The interaction energy of the "ghost" molecule with the remaining molecules (U_{ghost}) is evaluated and subsequently used for the calculation of the excess chemical potential (μ^{ex}) of the component:

$$\mu^{ex} = \mu - \mu^{ig} = -\frac{1}{\beta}\ln\left[\frac{1}{\langle V\rangle_{NPT}}\langle V\langle\exp(-\beta U^{\text{intra}}_{\text{ghost}} - \beta U^{\text{inter}}_{\text{ghost}})\rangle_{\text{Widom}}\rangle_{NPT}\right] + \frac{1}{\beta}\ln\langle\exp(-\beta U^{\text{intra}}_{\text{ghost}})\rangle_{\text{ideal gas}} \quad (3)$$

where $\beta = 1/kT$, $U^{\text{inter}}_{\text{ghost}}$ is the intermolecular energy and $U^{\text{intra}}_{\text{ghost}}$ is the intramolecular energy of the "ghost" molecule. The latter is calculated independently in a single chain simulation. V is the instantaneous volume of the system and the brackets denote ensemble averaging over all configurations and spatial averaging over all "ghost" molecule positions.

From the excess chemical potential, one may calculate the infinite dilution solubility coefficient S_o from the expression:

$$S_o = \frac{22400\ \text{cm}^3\ (\text{STP})/\text{mol}}{RT}\lim_{x_{solute}\to 0}\exp(-\beta\mu^{ex}_{solute}) \quad (4)$$

In this work S_o is reported in units of cm^3 (STP)/ (cm^3 atm). STP (widely used in membrane science) stands for standard temperature and pressure conditions and corresponds to an absolute pressure of 101.325 kPa and a temperature of 273.15 K.

NVT simulations were also performed for systems consisting of 3 PDMS chains of 80 monomer units each and a number of gas molecules (10 He, Ne or Ar, or 5 O_2 or N_2 molecules) or *n*-alkane molecules (10 CH_4 or 5 C_2H_6 up to *n*-C_6H_{14} molecules). Simulations were performed in the temperature range 300−450 K. Long simulation runs, corresponding to real time of 50−150 ns were executed in order to obtain reliable results. The self-diffusion coefficient was calculated from the linear part of the mean square displacement of the centers of mass of the solutes according to the Einstein equation:

$$D = \lim_{t\to\infty}\frac{1}{6}\frac{\mathrm{d}}{\mathrm{d}t}\langle|r_i(t) - r_i(0)|^2\rangle \quad (5)$$

The force fields parameters for the gases and *n*-alkanes examined here are the same as in our previous work.[31]

3. Results and Discussion

A. Validation of Model II for Structure and Thermodynamic Properties. The polymer melt density calculated at various temperatures and pressures with Model II agrees within statistical uncertainty with the calculations with Model I reported previously.[31] Similar good agreement between the two models was obtained for other thermodynamic properties (Hildebrand solubility parameter, thermal expansion coefficient, etc.) verifying that the torsional potential details have relatively little effect on the thermodynamic properties of polymer melts.

On the other hand, the increase of molecular chain flexibility (through reduction of k_ϕ) has significant effect on the dihedral angle distribution, as one might expect. In Figure 1, the probability density distribution of Si−O−Si-O dihedral angle of PDMS at 300 K as predicted from Models I and II is shown.

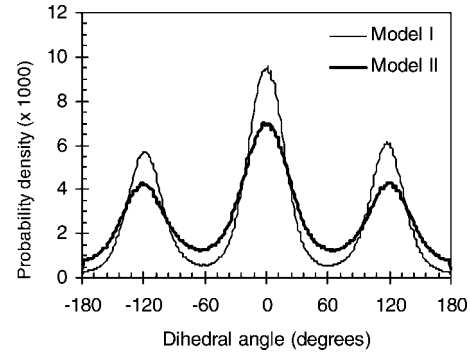

Figure 1. Probability density distribution of PDMS dihedral angles at 300 K from MD using Model I and Model II.

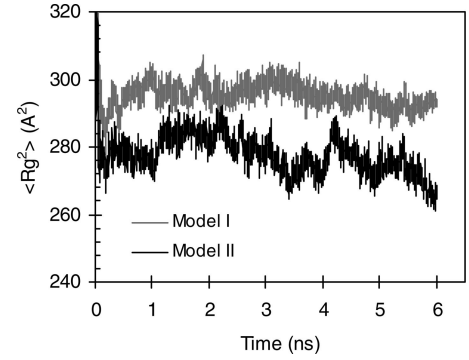

Figure 2. $\langle R_g^2\rangle$ evolution with time for PDMS melt at 300 K from Model I and Model II.

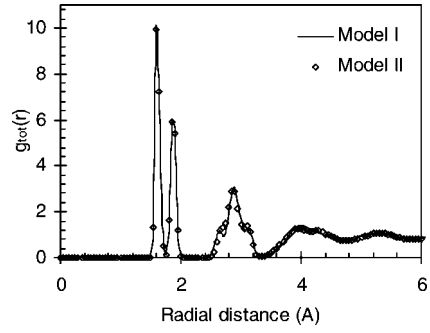

Figure 3. Total pair distribution function at 300 K and 0.1 MPa for PDMS from Model I and from Model II.

Model II results in a broader distribution of *trans, gauche*$^+$ and *gauche*$^-$ states over Model I while the relative fractions remain unchanged. No experimental data are available that could be possibly used to validate these predictions. The difference in the dihedral angle distribution results in different PDMS chain sizes. In Figure 2, the evolution of $\langle R_g^2\rangle$ values over time for PDMS at 300 K is presented. Model II chains exhibit a more compact structure. More specifically, simulation data reveal that $\langle R_g^2\rangle = (286 \pm 7)$ Å^2 for Model I and (268 ± 10) Å^2 for Model II.

The two models predict very similar local microscopic structure for the polymer melt that is quantified in terms of the total radial distribution function, g_{tot}(r), as shown in Figure 3. In our previous work,[31] Model I predictions were shown to be in very good agreement with experimental data and literature molecular simulation results for g_{tot}(r) using UA and explicit atom force fields for PDMS.

B. Local Chain Dynamics. The local dynamics of the chains was quantified in terms of the torsion angle autocorrelation

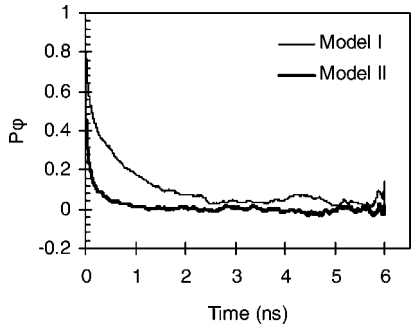

Figure 4. Torsion angle autocorrelation function for PDMS at 300 K from Model I and from Model II.

function as predicted from the two models, according to the expression:

$$P_{\phi}(t) = \frac{\langle \cos\phi(t)\cos\phi(0)\rangle - \langle\cos\phi(0)\rangle^2}{\langle\cos\phi(0)^2\rangle - \langle\cos\phi(0)\rangle^2} \quad (6)$$

The decay of $P_{\varphi}(t)$ for PDMS at 300 K is shown in Figure 4. Clearly, the local conformational relaxation of PDMS chains represented by Model II is faster compared to that obtained from Model I. The data were fitted to the Kohlrausch−Williams−Watts (KWW) equation:

$$P_{KWW}(t) = \exp\left(-\left(\frac{t}{\tau_c}\right)^{\beta}\right) \quad (7)$$

where τ_c is a characteristic decorrelation time and β is a stretching parameter. At 300 K, for Model I, $\tau_c = 305$ ps and $\beta = 0.49$ and for Model II, $\tau_c = 29$ ps and $\beta = 0.39$. Dihedral decorrelation time is evaluated from the expression:

$$\tau = \int_0^{\infty} P_{KWW}(t)\,\mathrm{d}t = \tau_c \frac{\Gamma\left(\frac{1}{\beta}\right)}{\beta} \quad (8)$$

Analysis of the simulation data, resulted in $\tau = 620$ ps for Model I and 100 ps for Model II, respectively.

C. Solubility Calculations. The infinite dilution solubility coefficient, S_o, for a number of light gases and *n*-alkanes in PDMS was calculated using the Widom test particle insertion methodology. In Table 1, simulation results from Model I and Model II at 300 K are presented together with available experimental data. In all cases, predictions from the two models essentially coincide within the statistical uncertainty of the calculations and are in very good agreement with experiment.

D. Self-Diffusion Coefficient Calculations. Long *NVT* MD simulations on the order of 100 ns each using both Models I and II were performed for the estimation of the diffusion coefficient of solutes in PDMS. At each state point, the same density value (equal to the value resulted from the *NPT* simulations for the PDMS−solute mixture at the same temperature and ambient pressure) was used using either of the two models. The solute diffusion coefficient, *D*, was calculated from the mean square displacement (msd) of solute molecules with time, according to the Einstein relation (Eq. 5). The criterion that a system has reached the normal diffusive regime is that a log(msd) - log(time) plot is a linear line with slope equal to 1. Furthermore, solute molecules should be displaced on average during the simulation by a distance greater than the size of the simulation box, to ensure that true diffusion is observed within simulation time.[39] In Figure 5, the number of simulation boxes traveled by three different solutes (He, CH_4 and *n*-C_6H_{14}) in PDMS as a function of time, obtained from Model II at 300 K, is displayed. Similar results were obtained from Model I. Apparently, He molecules are displaced faster compared to the other two solute molecules, due to their smaller size and weaker interactions with the polymer matrix. After 6 ns of simulation time, He has traveled a distance equivalent to 5 simulation boxes. On the other hand, CH_4 and *n*-C_6H_{14} molecules need about 100 ns to travel a distance equivalent to 6 and 3 simulation boxes, respectively.

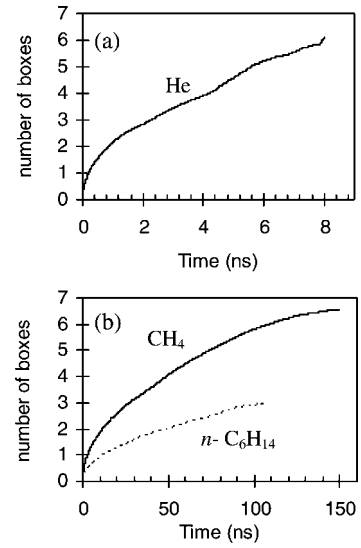

Figure 5. Number of boxes traveled by (a) He and (b) CH_4 and *n*-C_6H_{14} as a function of time in PDMS at 300 K.

Calculated and experimental diffusion coefficients of five gases (He, Ne, Ar, N_2 and O_2) in PDMS at 300 K, using the two models, are depicted in Table 2. Experimental data and model predictions are in full agreement concerning the order of *D* variation, for the inert gases that is: He > Ne > Ar and for the light gases that is: $O_2 > N_2$. *D* values for He, Ne, O_2 and N_2 in PDMS have been determined by Barrer and Chio[17]

Table 1. Calculated and Experimental Infinite Dilution Solubility Coefficients, S_o, of Light Gases and *n*-Alkanes in PDMS at 300 K

	S_o (cm^3 (STP)/cm^3 atm)		
component	Model I	Model II	experiment
He	0.044 ± 0.003	0.043 ± 0.002	0.028,[24] 0.046,[21] 0.043[17]
Ne	0.059 ± 0.003	0.057 ± 0.003	0.042[24]
Ar	0.23 ± 0.03	0.21 ± 0.01	0.256,[22] 0.225,[24] 0.34[17]
Kr	0.58 ± 0.04	0.62 ± 0.04	0.59[24]
Xe	2.1 ± 0.3	2.1 ± 0.2	1.92[24]
N_2	0.11 ± 0.02	0.10 ± 0.01	0.127,[22] 0.09,[25] 0.111,[24] 0.12,[23] 1.1[28]
O_2	0.17 ± 0.03	0.16 ± 0.01	0.224,[22] 0.18[25] 0.205[24]
CH_4	0.36 ± 0.02	0.36 ± 0.03	0.6,[19] 0.525,[22] 0.436,[24] 0.38,[28] 0.42,[25] 0.45,[20] 0.43[23]
C_2H_6	2.0 ± 0.1	1.9 ± 0.2	3.2,[19] 3.01,[22] 2.34,[24] 2.2[25]
C_3H_8	5.5 ± 0.2	5.8 ± 0.1	13.5,[20] 7.7,[19] 7.5,[24] 5.0,[25] 6.45[20]
n-C_4H_{10}	18 ± 1	17 ± 2	14,[19] 21.9,[24] 21.4[18]
n-C_5H_{12}	56 ± 12	48 ± 10	64.4,[24] 63.5,[29] 62.2[18]
n-C_6H_{14}	157 ± 91	135 ± 85	

Table 2. Calculated and Experimental Diffusion Coefficients, *D*, of Light Gases in PDMS at 300 K

	D ($\times 10^6$ cm^2 s^{-1})		
gas	Model I	Model II	experiment
He	55.7	63	52.5[17] 60[18]
Ne	20.5	28	21[17]
Ar	5.5	7	14[18]
O_2	4.5	9.5	19,[17] 16,[18] 34[25]
N_2	3.3	8.6	11.8,[17] 15,[18] 34[25]

Table 3. Diffusion Coefficient of *n*-Alkanes in PDMS at 300 K from Model I, Model II, and Experimental Data

	D ($\times 10^6$ cm^2 s^{-1})					
	CH_4	C_2H_6	C_3H_8	*n*-C_4H_{10}	*n*-C_5H_{12}	*n*-C_6H_{14}
			MD Simulation			
Model I	3	1.2	0.7	0.43	0.34	0.30
Model II	6	2.7	2.5	1.8	1.6	1.4
			Experiment			
Stern et al.[40]	24		10.1			
Merkel et al.[25]	22	11.3	5.1			
Krüger et al.[29]					5[a]/9[b]	
Yampolskii et al.[19]	11.3	6.2	4.2			
Raharjo et al.[30]	18			4.4		
LaPack et al.[41]	16	11	6.4	6.3	4.5	3.5

[a] Sorption balance measurement. [b] Pressure decay measurement.

using the time-lag method in the temperature range from 256 to 273 K. The values reported in Table 2 at 300 K were obtained by extrapolation, so that a direct comparison can be made with experimental data from other sources and from simulation. For the two lighter gases, both Model I and II predictions are in good agreement with experimental data; although Model I results are closer to the data. MD simulations for D of He in PDMS at 300 K have been reported previously by Sok et al.[7] and Charati and Stern[10] using a UA and an all atom force field, respectively. In both cases, He D was overestimated: Sok et al.[7] reported a value of $D = 180 \times 10^{-6}$ cm^2/s while Charati and Stern[10] reported a value of $D = 119 \times 10^{-6}$ cm^2/s.

As the solute molecular size increases, deviations between model predictions and experimental data increase. For the case of O_2 and N_2 where data from different sources are available, there is significant scatter in the reported values. In all cases, Model II predictions are larger than Model I predictions and closer to the experimental values. Furthermore, for larger solute molecules the difference between the two model predictions increases. Clearly, the model chain flexibility has a significant effect to the diffusion of penetrant molecules and this effect becomes more pronounced as the size of the penetrant molecules increases.

In Table 3 and Figure 6, experimental data[19,25,29,30,40,41] and MD simulation results for the diffusion coefficients of *n*-alkanes in PDMS at 300 K are presented. Predictions from both models are lower than experimental values which, in turn, exhibit significant scatter which is also a measure of the uncertainty associated with these measurements. For the case of *n*-C_5H_{12} Krüger et al.[29] used two different methods resulting in significantly different values: The pressure decay method provided a value of $D = 9 \times 10^{-6}$ cm^2/s while the sorption balance method a value of $D = 5 \times 10^{-6}$ cm^2/s. A comparison against the value reported by La Pack et al.[41] for *n*-C_5H_{12} and values for the lighter *n*-alkanes makes the latter value more realistic. In all cases, Model II predictions are closer to the experimental data than Model I predictions. In line with the conclusion for the gas calculations of Table 2, as the *n*-alkane size increases the difference between the two models increases: For CH_4, D from Model II is twice the value from Model I while for *n*-C_6H_{14} D from Model II is more than four times larger than from Model I.

In Figure 7, the temperature dependence of the diffusion

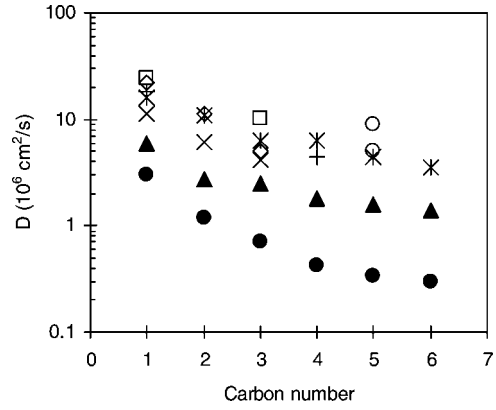

Figure 6. Diffusion coefficient of *n*-alkanes in PDMS. MD predictions using Model I (solid circles) and Model II (solid triangles). Experimental data: (×) from Yampolskii et al.,[19] (◇) from Merkel et al.,[25] (○) from Krüger et al.,[29] (+) from Raharjo et al.,[30] (□) from Stern et al.,[40] and (∗) from LaPack et al.[41]

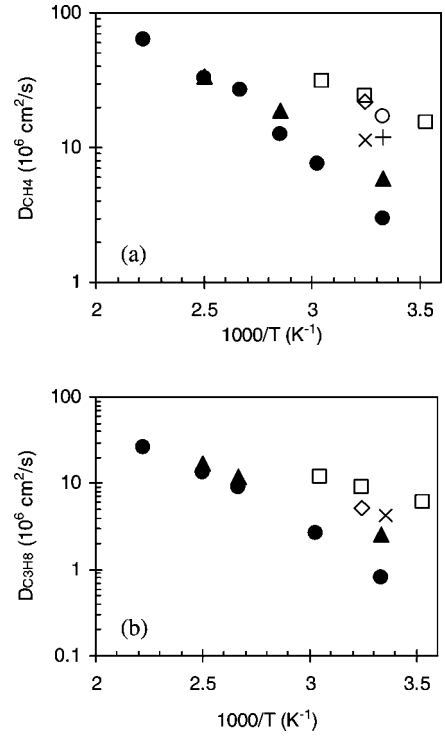

Figure 7. Temperature dependence of diffusion coefficient for (a) CH_4 and (b) C_3H_8 in PDMS. MD predictions obtained from Model I (solid circles) and from Model II (solid triangles). Experimental data: (+) from Robb et al.,[18] (×) from Yampolskii et al.,[19] (◇) from Merkel et al.,[25] (○) from Tremblay et al.,[28] and (□) from Stern et al.[40]

coefficient for CH_4 and C_3H_8 in the range 300−450 K is shown. MD results obtained from the two models are presented together with available experimental data.[18,19,25,28,40] For both penetrants, simulated and experimental values reveal an Arrhenius behavior. In all cases, for a given temperature the D value predicted by Model II is higher than the D value predicted by Model I. However, at elevated temperatures the difference between the two models decreases. It is concluded that the dependence of diffusion coefficient on chain flexibility is stronger at low temperatures, where the diffusion mechanism is relatively slower. The faster translational motion of the polymer chains at elevated temperatures and the relatively larger free volume available for diffusion of penetrant molecules contribute to the decrease of the difference between the two models.

Table 4. Activation Energy of Diffusion of CH_4, C_3H_8, and n-C_4H_{10} in PDMS

	activation energy of diffusion (kJ/mol)		
solute	Model I	Model II	experiment
CH_4	23.0	17.6	12.6,[30] 12.1[40]
C_3H_8	24.8	19.1	7 ± 1.2,[27] 11.8[40]
n- C_4H_{10}	32.7	18.8	17 ± 3,[30] 18[42]

The activation energy of diffusion for CH_4, C_3H_8, and n-C_4H_{10} in PDMS was calculated from the Arrhenius relation:

$$D = D_o \exp\left(-\frac{E_d}{RT}\right) \tag{9}$$

where D_o is a constant, E_d is the activation energy, and R is the ideal gas constant. Results are shown in Table 4 together with experimental data. As expected based on the data of Figure 7, Model II predicts a lower activation energy compared to Model I. Interestingly, Model I predicts a substantial increase of activation energy for higher n-alkanes, while Model II predictions are practically independent of the n-alkane size. Prediction from Model II is in excellent agreement with the experimental data for n-C_4H_{10} and in fair agreement with experiments for CH_4 and C_3H_8.

The effect of penetrant concentration on the diffusion coefficient value was examined. MD simulations for PDMS−CH_4 and PDMS−n-C_4H_{10} mixtures at 350 K and various compositions were performed. In all cases, Model I was used for PDMS. Simulations were performed in the *NVT* ensemble and mass density was kept constant for a given mixture, independent of composition. For the PDMS−CH_4 mixture, the density was set equal to 0.903 g/cm^3 and for the PDMS−n-C_4H_{10} mixture it was set equal to 0.912 g/cm^3, corresponding to the equilibrium density obtained from *NPT* simulations for 1 wt % CH_4 mixture and 2 wt % n-C_4H_{10} mixture at 0.1 MPa, respectively. In Figure 8, D values for CH_4 and n-C_4H_{10} are presented as a function of the penetrant weight fraction. In both cases, the diffusion coefficient increases with penetrant concentration. It has been reported previously that the diffusion coefficient of supercritical gases are independent of the gas concentration, while for subcritical solutes, which are more soluble in polymers, the diffusion coefficient may increase rapidly with increasing concentration.[43] Experimental measurements by Sato et al.[44] revealed a weak positive concentration dependence on the diffusion coefficient of N_2 in poly(propylene) and of N_2 and CO_2 in high density poly(ethylene) at 453 K. Moreover, recent MD calculations by Faure et al.[45] showed an increase in the diffusion coefficient of CO_2 and H_2S in poly(ethylene) at 433 K with increasing penetrant weight fraction up to approximately 0.15.

E. Permeability and Separation Factor Calculations. The permeability of a polymer to a given penetrant is calculated as the product of solubility coefficient and the diffusion coefficient,

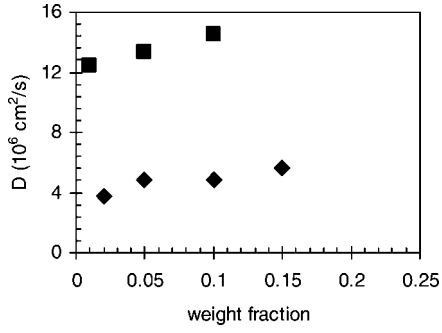

Figure 8. Diffusion coefficient of CH_4 (squares) and n-C_4H_{10} (diamonds) in PDMS at 350 K as a function of solute weight fraction calculated by MD simulations using Model I.

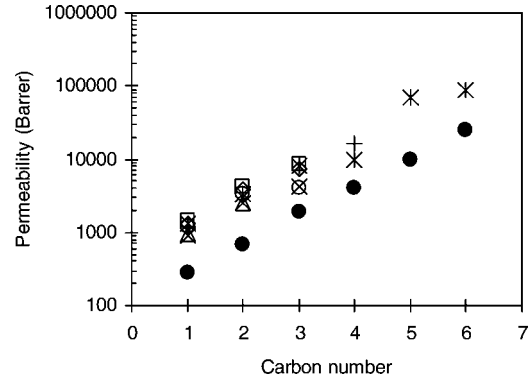

Figure 9. Permeability of n-alkanes in PDMS at 300 K. MD predictions using Model II (solid circles). Experimental data: (Δ) from Robb et al.,[18] (×) from Yampolskii et al.,[19] (○) from Merkel et al.,[25] (+) from Raharjo et al.,[30] (□) from Stern et al.,[40] (∗) from LaPack et al.,[41] and (◇) from Pinnau et al.[47]

$P = S \times D$. In Figure 9, experimental data[18,19,25,30,40,41,47] and molecular simulation results are shown for the permeability of PDMS to n-alkanes at 300 K. Clearly, simulation results are consistently lower than experimental values for which significant scatter is observed concerning data from different sources. The deviation between experimental data and simulation is driven by the under-prediction of the diffusion coefficient of n-alkanes in PDMS.

Separation of a binary mixture of components i and j (where i is typically the most permeable of the two components) by a given polymer membrane is characterized by the ideal separation factor, which is the ratio of permeabilities for components i and j according to the expression:

$$\alpha_{ij}^{id} = \frac{P_i}{P_j} = \left(\frac{S_i}{S_j}\right)\left(\frac{D_i}{D_j}\right) \tag{10}$$

where the ratios $\alpha_{ij}^S = S_i/S_j$ and $\alpha_{ij}^D = D_i/D_j$ represent the solubility selectivity and the diffusivity selectivity, respectively. In rubbery polymers α_{ij}^D is less than unity, while $\alpha_{ij}^S \gg 1$, so ideal separation factor is governed by selectivity of sorption.[46] PDMS is a widely used polymer membrane and so ideal separation factors for various binary gas and liquid mixtures have been measured. Experimental data[18,25,30,40,41,47,48] and MD predictions for a number of n-alkane/CH_4 mixtures at 300 K are reported in Table 5 in terms of the three different selectivity ratios. For a given binary mixture, experimental data from different sources exhibit significant scatter. Predictions from Model II are in very good agreement with available experimental data for all three ratios. For the permeability selectivity and diffusivity selectivity, predictions from Model I are lower than predictions from Model II and from experiments while for the solubility selectivity the two models provide similar results.

The separation factor for n-C_4H_{10}/CH_4 mixture is used widely as a benchmark for hydrocarbon mixture separation capability of a given membrane material. In Figure 10, pure gas n-C_4H_{10}/CH_4 solubility, diffusivity and permeability selectivities in the range 273−400 K together with experimental data from Raharjo et al.[30] are shown. Solubility selectivity decreases significantly as temperature increases. Predictions obtained from Model I and Model II are in excellent agreement with experiments over the entire temperature range. The picture is different for the case of diffusivity selectivity for which experimental data in the temperature range 273−323 K exhibit an insignificant temperature effect. In this case, Model II predictions are in very good agreement with experimental data, although a weak temperature increase is predicted over a larger temperature range. Model I predicts a strong temperature effect which clearly disagrees with Model II and with experiments. The temperature

Table 5. Molecular Simulation Predictions and Experimental Values for the Ideal Permeability Selectivity, Solubility Selectivity and Diffusivity Selectivity of *n*-Alkane/CH_4 Pairs in PDMS at 300 K

	P(i)/P(CH_4)			S(i)/S(CH_4)			D(i)/D(CH_4)		
penetrant (i)	Model I	Model II	experiment	Model I	Model II	experiment	Model I	Model II	experiment
C_2H_6	2.2	2.3	3[a]/2.7[b]/2.6[f]/2.5[g]	5.5	5.3	5.2[b]/3.8[g]	0.40	0.45	0.5[b]/0.68[g]
C_3H_8	3.5	6.7	5.7[a]/3.4[b]/5.9[c]/6.2[g]	15.3	17	14.4[c]/12[b]/16.4[g]	0.23	0.42	0.41[c]/0.23[b]/0.4[g]
n-C_4H_{10}	7.2	14	14.8[d]/18[e] /9.5[f]/7.7[g]	50	47	54[d]/26[f]/20[g]	0.14	0.30	0.28[d]/0.4[f]/0.4[g]
n-C_5H_{12}	18	34	21[f]/53[g]	155	133	190[g]	0.11	0.26	0.28[g]
n-C_6H_{14}	44	86	68[g]	436	375	316[g]	0.10	0.23	0.22[g]

[a] Taken from ref 47. [b] Taken from ref 25. [c] Taken from ref 40. [d] Taken from ref 30. [e] Taken from ref 48. [f] Taken from ref 18. [g] Taken from ref 41.

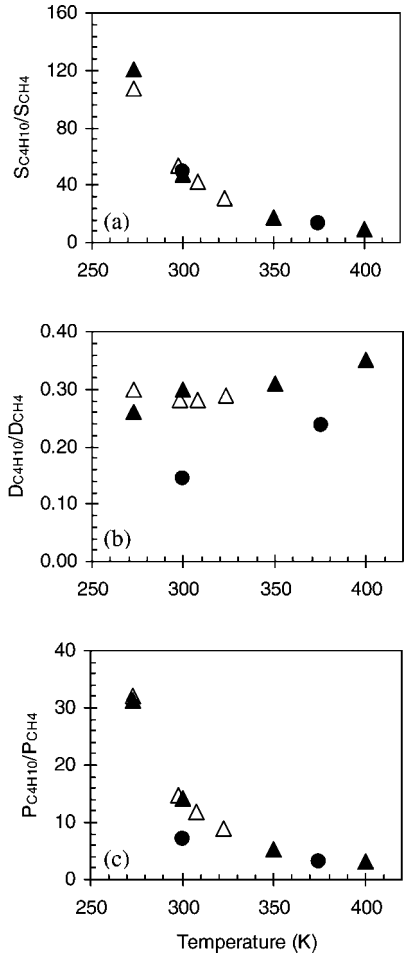

Figure 10. Effect of temperature on pure *n*-C_4H_{10}−CH_4 (a) solubility, (b) diffusivity, and (c) permeability selectivity. Solid circles were obtained from Model I, solid triangles from Model II and open triangles are experimental data reported by Raharjo et al.[30]

variation in permeability selectivity (or separation factor) is driven by the variation exhibited in solubility selectivity. Accordingly, Model II remains in excellent agreement with experimental data while Model I deviates from experiment, especially at lower temperatures.

A quantitative picture regarding the temperature effect on ideal solubility, ideal diffusivity and ideal permeability selectivity of PDMS for the binary *n*-C_4H_{10}−CH_4 is given in Table 6 based on Model II simulation results. As temperature increases, both S_{CH_4} and $S_{n\text{-}C_4H_{10}}$ decrease with a rate that is much higher for the latter. Furthermore, a temperature increase results in increase for D_{CH_4} and $D_{n\text{-}C_4H_{10}}$, with a similar rate. Finally, P_{CH_4} increases while $P_{n\text{-}C_4H_{10}}$ decreases with temperatures. These predictions are consistent with available experimental data.[30,47] On the other hand, Model I predicts an increase for both P_{CH_4} and $P_{n\text{-}C_4H_{10}}$ with temperature (not shown here).

F. Simulation Results for Penetrant Mixtures. For the accurate design of a polymer membrane for the separation of a real mixture, mixture permeability data are needed. Significant experimental and simulation work has been devoted to the permeability and diffusivity of mixed gases in polymers.[45,49–56] It is often assumed that in rubbery polymers penetrants permeate independently of one another.[55] However, this behavior needs to be confirmed for a given system. Recent experimental data[30] for the *n*-C_4H_{10} - CH_4 mixture in PDMS showed an increase in CH_4 solubility in the presence of *n*-C_4H_{10} in the polymer. On the other hand, only a weak influence of CH_4 on *n*-C_4H_{10} solubility was reported.

In this work, molecular simulation sorption calculations were performed for this ternary mixture. More specifically, the infinite dilution solubility coefficient of CH_4 in a PDMS−*n*-C_4H_{10} mixture was examined. Three different mixtures were simulated consisting of 3 PDMS chains of 80 monomer units each with a *n*-C_4H_{10} weight fraction equal to 0.10, 0.13, and 0.20, respectively. *NPT* simulations of PDMS−*n*-C_4H_{10} mixtures at 300 and 450 K were performed lasting 6 ns each and the resulting configurations were used for CH_4 molecule insertions in order to calculate the infinite dilution solubility coefficient of the latter with the Widom particle insertion method. Results depicted in Figure 11 indicate that at both temperatures, CH_4 solubility increases as *n*-C_4H_{10} concentration in the polymer increases. For example, at 300 K S_o of CH_4 increases from 0.36 cm^3 (STP)/cm^3 atm (0 wt % *n*-C_4H_{10}) to 0.51 cm^3 (STP)/cm^3 atm (20 wt % *n*-C_4H_{10}). Clearly, the presence of *n*-C_4H_{10} molecules in the polymer creates a more favorable environment for CH_4 sorption, which enhances CH_4 solubility. This behavior is consistent with the recent experimental data of Raharjo et al.[30] at 298 K shown in Figure 11.

The diffusion coefficients of a mixture of gases, CH_4 and *n*-C_4H_{10}, in PDMS at ambient conditions were also calculated and compared to pure gas diffusion calculations. Two systems were examined containing (a) 3 PDMS chains of 80 monomer units each + 1 wt % CH_4 (10 CH_4 molecules) + 2 wt % *n*-C_4H_{10} (5 C_4H_{10} molecules) and (b) 3 PDMS chains of 80 monomer units each + 1 wt % CH_4 (10 CH_4 molecules) + 10 wt % *n*-C_4H_{10} (27 C_4H_{10} molecules), respectively. *NPT* simulations of 50 − 100 ns were performed at 300 K and 0.1 MPa using Model II for PDMS. In Figure 12, mixed gas *D* predictions together with pure gas *D* predictions are displayed. Clearly, CH_4 molecules move faster in the presence of *n*-C_4H_{10} molecules in PDMS matrix than in pure polymer. The same behavior is observed for *n*-C_4H_{10} in the presence of CH_4 molecules. The presence of a second penetrant species swells the polymer matrix resulting in an increase in the diffusion coefficient of the first penetrant. For example, pure CH_4 diffusion coefficient of 6×10^{-6} cm^2/s corresponds to density of 0.942 g/cm^3. The presence of 10 wt % *n*-C_4H_{10} in the polymer decreases density to 0.899 g/cm^3 and approximately doubles CH_4 diffusion coefficient value. On the other hand, the presence of 1 wt % CH_4 in polymer caused a slightly decrease in system density from 0.942 g/cm^3 to 0.928 g/cm^3 and an increase in *n*-C_4H_{10} diffusion coefficient from 1.8×10^{-6} cm^2/s to 2.6×10^{-6} cm^2/s.

Table 6. Temperature Dependence of Pure CH_4 and n-C_4H_{10} Solubility, Diffusivity, and Permeability in PDMS and of Corresponding n-C_4H_{10}−CH_4 Selectivities Obtained from Model II[a]

T	S_{CH_4}	D_{CH_4}	P_{CH_4}	$S_{n\text{-}C_4H_{10}}$	$D_{n\text{-}C_4H_{10}}$	$P_{n\text{-}C_4H_{10}}$	$S_{n\text{-}C_4H_{10}}/S_{CH_4}$	$D_{n\text{-}C_4H_{10}}/D_{CH_4}$	$P_{n\text{-}C_4H_{10}}/P_{CH_4}$
273	0.44	2.3	133	53	0.6	4184	120	0.26	31.4
300	0.36	6.0	284	17	1.8	4026	47	0.30	14.2
350	0.26	19.0	650	4.5	6.0	3552	17.2	0.31	5.4
400	0.22	33.7	975	2.0	11.8	3105	9.2	0.35	3.2

[a] Units: T (K), S (cm^3 (STP)/cm^3 atm), D (10^{-6} cm^2/s), and P (Barrer).

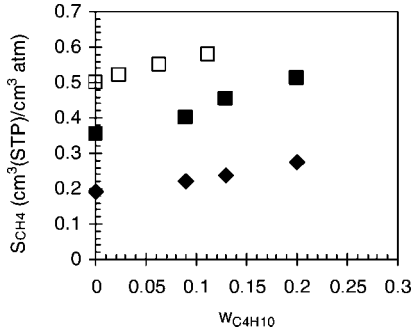

Figure 11. Mixed gas CH_4 solubility in PDMS at 300 K (solid squares) and 450 K (solid diamonds) as a function of n-C_4H_{10} weight fraction in PDMS predicted by molecular simulation. Open squares are experimental data[30] at 298 K.

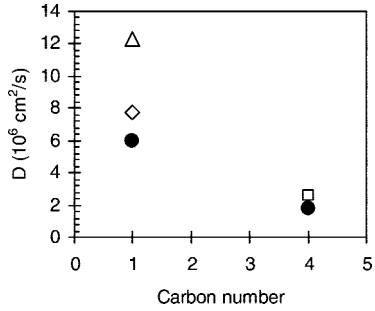

Figure 12. Diffusion coefficient of pure and mixed n-alkanes in PDMS at ambient conditions. Solid circles correspond to pure CH_4 and n-C_4H_{10} diffusion coefficient in PDMS. Values corresponding to n-alkanes in mixture: (◇) CH_4 mixed with 2% n-C_4H_{10} in PDMS, (△) CH_4 mixed with 10% n-C_4H_{10} in PDMS, and (□) n-C_4H_{10} mixed with 1% CH_4 in PDMS.

The swelling behavior of PDMS in the presence of mixed gases and the consequent increase in diffusivity and permeability coefficients of the corresponding gases has also been reported experimentally by other investigators.[30,47,56] Raharjo et al.[30] as well as Pinnau et al.[47] reported CH_4 - n-C_4H_{10} mixed gas permeability in PDMS and observed an increase in both gas permeabilities due to swelling. Moreover, Jordan and Koros[56] reported an increase in CH_4 and N_2 permeability in PDMS in CO_2−CH_4 and CO_2−N_2 mixtures, respectively, due to the plasticization of the PDMS matrix from the highly sorbing CO_2.

4. Conclusions

The permeability properties of PDMS to light gases and to n-alkanes were calculated by molecular simulation using a recently proposed UA force field that was tuned to structure and thermodynamic properties of PDMS melt. The polymer chain flexibility affects significantly the diffusion of penetrant molecules in the polymer matrix. Using two different values for the force constant ($k_\phi = 1.8$ and 0.9 kcal/mol, respectively) in the torsional potential that controls the chain stiffness, significant differences were obtained for the diffusion coefficient that increase with penetrant size. At 300 K, D values with the two force fields differ by 13% for He, by 100% for CH_4 and up to 350% for n-C_6H_{14}. In all cases, the lower force constant (Model II) results in better agreement with available experimental data over the higher force constant (Model I). The force constant variation affects primarily the local chain dynamics while it has an insignificant effect on the solubility coefficient of gases and n-alkanes in the polymer melt.

Permeability coefficients and separation factors (selectivities) were calculated for various n-alkane and binary n-alkane mixtures, respectively. Predictions concerning the former are systematically lower than experimental data, due to lower diffusion coefficient predictions. Model II results in excellent prediction of selectivities over a wide temperature range.

Finally, molecular simulations were performed for binary penetrant mixtures with PDMS. The presence of a second penetrant increases both the solubility coefficient and the diffusion coefficient of the first penetrant species, in agreement with limited experimental data available. In summary, molecular simulation using detailed atomistic force fields is a powerful tool for the elucidation of structure and prediction of permeability properties of rubbery polymers, in most cases in good agreement with experimental data.

Acknowledgment. Financial support of this project through the European Union−European Social Fund, the Greek Secretariat of Research and Technology, and Bayer Technology Services GmbH is gratefully acknowledged. We are thankful to Prof. Dr. Ralf Dohrn and Dr. Oliver Pfohl of Bayer Technology Services GmbH, Germany, for helpful discussions regarding this work, to Dr. Philippe Ungerer of IFP, France, for suggestions regarding the force field development and to Prof. Benny Freeman of University of Texas at Austin, TX, for providing his manuscripts prior to publication.

References and Notes

(1) Vrentas, J. S.; Duda, J. L. *J. Polym. Sci., Polym. Phys.* **1977**, *15*, 403.
(2) Cohen, M. H.; Turnbull, D. *J. Chem. Phys.* **1959**, *31*, 1164.
(3) Vrentas, J. S.; Duda, J. L.; Ling, H.-C.; Hou, A.-C. *J. Polym. Sci., Polym. Phys.* **1985**, *23*, 289.
(4) Takeuchi, H.; Okazaki, K. *J. Chem. Phys.* **1990**, *92*, 5643.
(5) Takeuchi, H. *J. Chem. Phys.* **1990**, *93*, 2062.
(6) Müller-Plathe, F. *J. Chem. Phys.* **1991**, *94*, 3192.
(7) Sok, R. M.; Berendsen, H. J. C.; van Gunsteren, W. F. *J. Chem. Phys.* **1992**, *96*, 4699.
(8) Tamai, Y.; Tanaka, H.; Nakanishi, K. *Macromolecules* **1994**, *27*, 4498.
(9) Gee, R. H.; Boyd, R. H. *Polymer* **1995**, *36*, 1435.
(10) Charati, S. G.; Stern, S. A. *Macromolecules* **1998**, *31*, 5529.
(11) Hahn, O.; Mooney, D. A.; Muller-Plathe, F.; Kremer, K. *J. Chem. Phys.* **1999**, *111*, 6061.
(12) Meunier, M. *J. Chem. Phys.* **2005**, *123*, 134906.
(13) Alentiev, A.; Economou, I. G.; Finkelshtein, E.; Petrou, J.; Raptis, V. E.; Sanopoulou, M.; Soloviev, S.; Ushakov, N.; Yampolskii, Y. *Polymer* **2004**, *45*, 6933.
(14) Harmandaris, V. A.; Adhikari, N. P.; van der Vegt, N. F. A.; Kremer, K.; Mann, B. A.; Voelkel, R.; Weiss, H.; Liew, C. C. *Macromolecules* **2007**, *40*, 7026.
(15) Raptis, T. E.; Raptis, V. E.; Samios, J. *J. Phys. Chem. B* **2007**, *111*, 13683.
(16) Hofmann, D.; Fritz, L.; Ulbrich, J.; Schepers, C.; Böhning, M. *Macromol. Theory Simul.* **2000**, *9*, 293.
(17) Barrer, R. M.; Chio, H. T. *J. Polym. Sci. C* **1965**, *10*, 111.
(18) Robb, W. L. *Ann. N.Y. Acad. Sci.* **1968**, *146*, 119.
(19) Yampolskii, Y.; Durgaryan, S. G.; Nametkin, N. S. *Vysokomol Soed, B* **1979**, *21*, 616.
(20) Shah, V. M.; Hardy, B. J.; Stern, S. A. *J. Polym. Sci., B: Polym. Phys* **1986**, *24*, 2033.

(21) Pauly, S. In *Polymer Handbook*, 3rd ed.; Brandrup, J. Immergut, E. H., Eds.; Wiley: New York, 1989.
(22) Kamiya, Y.; Naito, Y.; Hirose, T.; Mizoguchi, K. *J. Polym. Sci., B: Polym. Phys.* **1990**, *28*, 1297.
(23) Pope, D. S.; Sanchez, I. C.; Koros, W. J.; Fleming, G. K. *Macromolecules* **1991**, *24*, 1779.
(24) Kamiya, Y.; Naito, Y.; Terada, K.; Mizoguchi, K.; Tsuboi, A. *Macromolecules* **2000**, *33*, 3111.
(25) Merkel, T. C.; Bondar, V. I.; Nagai, K.; Freeman, B. D.; Pinnau, I. *J. Polym. Sci., B: Polym. Phys.* **2000**, *38*, 415.
(26) Pfohl, O.; Riebesell, C.; Dohrn, R. *Fluid Phase Equilib.* **2002**, *202*, 289.
(27) Prabhakar, R. S.; Merkel, T. C.; Freeman, B. D.; Imizu, T.; Higuchi, A. *Macromolecules* **2005**, *38*, 1899.
(28) Tremblay, P.; Savard, M. M.; Vermette, J.; Paquin, R. *J. Membr. Sci.* **2006**, *282*, 245.
(29) Krüger, K-M.; Pfohl, O.; Dohrn, R.; Sadowski, G. *Fluid Phase Equilib.* **2006**, *241*, 138.
(30) Raharjo, R. D.; Freeman, B. D.; Sanders, E. S. *J. Membr. Sci.* **2007**, *292*, 45.
(31) Makrodimitri, Z. A.; Dohrn, R.; Economou, I. G. *Macromolecules* **2007**, *40*, 1720.
(32) Allen, M. P.; Tildesley, D. J. *Computer Simulation of Liquids*; Oxford Science Publications: Oxford, U.K., 1987.
(33) Nosé, S.; Klein, M. L. *Mol. Phys.* **1983**, *50*, 1055.
(34) Gear, C. W. *Numerical Initial Value Problems in Ordinary Differential Equations*; Prentice-Hall: Englewood Cliffs, NJ, 1971.
(35) Berendsen, H. J. C.; Postma, J. P. M.; van Gunsteren, W. F.; DiNola, A.; Haak, J. R. *J. Chem. Phys.* **1984**, *81*, 3684.
(36) Details can be found at www.accelrys.com/cerius2/.
(37) Theodorou, D. N.; Boone, T. D.; Dodd, L. R.; Mansfield, K. F. *Macromol. Chem., Theory Simul.* **1993**, *2*, 191.
(38) Widom, B. *J. Chem. Phys.* **1963**, *39*, 2808.
(39) June, R. L.; Bell, A. T.; Theodorou, D. N. *J. Chem. Phys.* **1991**, *95*, 8866.
(40) Stern, S. A.; Shah, V. M.; Hardy, B. J. *J. Polym. Sci., Part B: Polym. Phys.* **1987**, *25*, 1263.
(41) LaPack, M. A.; Tou, J. C.; McGuffin, V. L.; Enke, C. G. *J. Membr. Sci.* **1994**, *86*, 263.
(42) Barrer, R. M.; Barrie, J. A.; Raman, N. K. *Polymer* **1962**, *3*, 595.
(43) Stern, S. A.; Krishnakumar, B.; Nadakatti, S. M. Permeability of polymers to gases and vapors. In *Physical Properties of Polymers Handbook*; Mark, J. E., Ed.; AIP: Woodbury, NY, 1996; Chapter 50.
(44) Sato, Y.; Fujiwara, K.; Takikawa, T.; Takishima, S.; Masuoka, H. *Fluid Phase Equilib.* **1999**, *162*, 261.
(45) Faure, F.; Rousseau, B.; Lachet, V.; Ungerer, P. *Fluid Phase Equilib.* **2007**, *261*, 168.
(46) Yampolskii, Yu., Pinnau, I., Freeman, B. D., Eds. *Materials Science of Membranes for Gas and Vapor Separation*; Wiley: Chichester, U.K., 2006.
(47) Pinnau, I.; He, Z. *J. Membr. Sci.* **2004**, *244*, 227.
(48) Schultz, J.; Peinemann, K.-V. *J. Membr. Sci.* **1996**, *110*, 37.
(49) Fritz, L.; Hofmann, D. *Polymer* **1997**, *38*, 1035.
(50) Singh, A.; Freeman, B. D.; Pinnau, I. *J. Polym. Sci., Part B: Polym. Phys.* **1998**, *36*, 289.
(51) Dhingra, S. S.; Marand, E. *J. Membr. Sci.* **1998**, *141*, 45.
(52) Yeom, C. K.; Lee, S. H.; Lee, J. M. *J. Appl. Polym. Sci.* **2000**, *78*, 179.
(53) Merkel, T. C.; Gupta, R. P.; Turk, B. S.; Freeman, B. D. *J. Membr. Sci.* **2001**, *191*, 85.
(54) Raharjo, R. D.; Freeman, B. D.; Paul, D. R.; Sarti, G. C.; Sanders, E. S. *J. Membr. Sci.* **2007**, *306*, 75.
(55) Koros, W. J.; Chern, R. T.; Stannett, V.; Hopfenberg, H. B. *J. Polym. Sci., Polym. Phys. Ed.* **1981**, *19*, 1513.
(56) Jordan, S. M.; Koros, W. J. *J. Polym. Sci., B: Polym. Phys.* **1990**, *28*, 795.

MA800650U